JACS
JOURNAL OF THE AMERICAN CHEMICAL SOCIETY

ARTICLE

pubs.acs.org/JACS

Hydrogen Reactivity of Palladium Nanoparticles Coated with Mixed Monolayers of Alkyl Thiols and Alkyl Amines for Sensing and Catalysis Applications

Monica Moreno,[†] Francisco J. Ibañez,[‡] Jacek B. Jasinski,[§] and Francis P. Zamborini*[,†]

[†]Department of Chemistry and [§]Conn Center for Renewable Energy Research, University of Louisville, Louisville, Kentucky 40292, United States

[‡]Instituto de Investigaciones Fisicoquímicas Teóricas y Aplicadas (INIFTA), Universidad Nacional de La Plata-CONICET, Sucursal 4 Casilla de Correo 16 (1900), La Plata, Argentina

Supporting Information

ABSTRACT: Palladium monolayer-protected clusters (MPCs) coated with octylamines ($C8NH_2$), hexanethiolates (C6S), and mixed monolayers of $C8NH_2$ and C6S exhibit significantly different reactivities with hydrogen gas, depending on the relative amounts of the two ligands coating the Pd nanoparticle surface, as determined by UV−vis spectroscopy of Pd MPCs in solution and electronic measurements of films of Pd MPCs as a function of exposure time to hydrogen. The average estimated composition of the ∼3.0 nm diameter Pd MPCs was $Pd_{919}(C6S)_{192}$ or $Pd_{919}(C8NH_2)_{177-x}(C6S)_x$, where x was varied to be 0, 3, 10, 16, 32, or 81 by the synthesis of pure $C8NH_2$ Pd MPCs and subsequent liquid-phase place exchange with a varied amount of C6SH. When x = 0−10, the Pd MPCs react strongly with H_2, leading to aggregated particles in solution and large irreversible changes in the morphology of films accompanied by an increase in film conductivity by 2−5 orders of magnitude. $Pd_{919}(C6S)_{192}$ MPCs are stable against significant aggregation in solution and do not exhibit large film morphology changes, but they are also not highly reactive to H_2, as determined by minimal changes in the optical properties of solutions and the small, irreversible changes in the conductivity of films in the presence of H_2. Finally, when x is 32 and 81, the Pd MPCs are fairly stable, exhibit minimal aggregation or morphology changes, and readily react with H_2 based on the significant, reversible changes in film conductivity in the presence of H_2. Pd MPCs with mixed monolayers have the benefit of high H_2 reactivity while maintaining the structural stability necessary for sensing and catalysis applications.

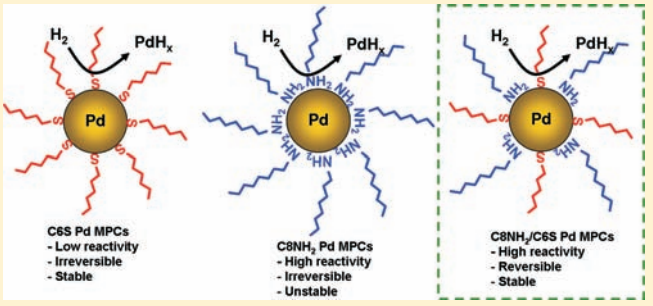

INTRODUCTION

Here we describe the reactivity between hydrogen and solutions or films of palladium monolayer-protected clusters (MPCs) coated with mixed monolayers of hexanethiolate (C6S) and octylamine ($C8NH_2$) ligands. This work is a follow up on our previous reports on the reactivity between hydrogen and pure C6S Pd, $C8NH_2$ Pd, $C12NH_2$ Pd, and $C16NH_2$ Pd MPCs, tetraoctylammonium bromide (TOABr)-stabilized Pd nanoparticles, and PdAu (10:1) or PdAg (10:1) alloys stabilized with C6S, $C8NH_2$, $C12NH_2$, or TOABr.[1,2] Our main goal is to control the reactivity between hydrogen and Pd-containing nanoparticles by controlling the metal and ligand composition of the nanoparticles for possible hydrogen sensing, storage, and catalysis applications. We previously showed that solid-state films of C6S Pd MPCs do not readily react well with hydrogen without prior ozone or heat treatment and that $C8NH_2$ Pd and $C12NH_2$ Pd MPCs react readily to the point of irreversible nanoparticle aggregation (i.e., unstable). We undertook this study based on our hypothesis that mixed monolayers of the two ligands would allow the benefit of both high reactivity and stability in the presence of hydrogen.

Hydrogen is light, clean, abundant, and sustainable.[3,4] It has been used in large quantities in a wide range of industries including chemical, food,[5,6] and glass processing and is a byproduct of steel making.[7] There is also a tremendous interest in hydrogen as a chemical energy source.[8] The low-cost production and ability to separate, purify,[9] store,[6,10] and manipulate hydrogen efficiently and safely would greatly benefit fuel cell technology, improving its potential to compete with traditional fossil fuels as an alternative energy source. There are safety concerns since hydrogen is highly explosive above 4% in air, requiring the development of hydrogen sensors. High capacity, effective, and reusable hydrogen storage materials are needed for energy applications since hydrogen suffers from low volumetric density.[6] These are some of the key challenges in the development of a hydrogen economy that Pd nanostructures may be able to address.

It is well-known that hydrogen adsorbs and dissociates spontaneously onto group VIII transition metals.[3,7] Among the many types of metals, the reaction between hydrogen and Pd or

Received: September 16, 2010
Published: February 25, 2011

dx.doi.org/10.1021/ja108378x | J. Am. Chem. Soc. 2011, 133, 4389–4397

Pd alloys has attracted a great deal of attention due to its relevance in applications in hydrogen sensing and storage and in catalysis.[11−13] The adsorption of hydrogen occurs in a two-step process involving the reversible adsorption of hydrogen molecules at the Pd surface, followed by rapid dissociation and diffusion of atomic hydrogen into the metal lattice, where it occupies octahedral interstitial sites with an increase in the lattice constant.[7] At low hydrogen partial pressures α-phase PdH_x forms, which becomes β-phase PdH_x at higher pressures.[14] The phase transition and associated increase in lattice constant alters the physical,[15,16] electrical,[17−34] and optical[35−38] properties of Pd and its alloys, forming the basis for hydrogen sensors.[39,40] The diffusion of hydrogen into the Pd lattice provides large hydrogen storage capacity, and the dissociation of hydrogen into the more active atomic hydrogen leads to its desirable catalytic properties.

Pd nanomaterials have been widely used as resistor-based hydrogen sensors.[40,41] The sensing mechanism relies on a change in resistance of the Pd nanostructure or nanostructured film upon exposure to hydrogen. For example, hydrogen sensors fabricated with well-connected Pd films show an increase in resistance in the presence of hydrogen due to the formation of the more resistive PdH_x material.[11,29,33] In contrast, films or nanostructures that contain high-resistance break junctions or discontinuities exhibit a decrease in resistance in the presence of hydrogen due to the volume enhancement of the material, leading to improved connectivity.[1,2,21−23,26,31,32,34,42] A third mechanism involves Schottky contacts formed by depositing Pd nanoparticles on n-type semiconductors (e.g., GaN,[3] GaAs,[18] SnO_2,[24,27] carbon nanotubes,[30] InP,[43] and DNA),[44] where the formation of PdH_x lowers the Schottky barrier height and increases the device current. In general, chemiresistive hydrogen sensors based on Pd nanostructures are promising due to their simplicity, high sensitivity and selectivity, reversibility, and low cost and portability.[1,3,39]

The capacity of Pd as a hydrogen-storage metal is given by the miscibility gap between the hydrogen solubilities of the α- and β-phases.[45] The benefits of storing hydrogen in the form of metal hydrides include high volume efficiencies, relative ease of recovery, indefinite storage capabilities without loss of hydrogen, and high degree of safety.[6] To date, many groups reported that the hydrogen storage properties of Pd nanoparticles are different from those of their bulk counterparts,[46−49] which is attributed to the large surface fraction in the particles and discreteness of their electronic states.[50] The hydrogen solubility increases in the α-phase but decreases in the β-phase, exhibiting miscibility gaps narrower than those compared to bulk Pd,[51] implying that Pd nanoparticles have fast kinetics for hydrogen decomposition/reformation on the metal surface and higher storage density in the inside/outside of the particles.[50] Several groups recently investigated the hydrogen sorption properties of Pd nanoparticles embedded into crystallized porous coordination polymers, also labeled metal−organic frameworks (MOFs),[10,52−54] demonstrating enhanced hydrogen uptake at room temperature due to the presence of the Pd nanoparticles incorporated into the pores of the polymer. Yamauchi and co-workers demonstrated the size dependence of the hydrogen storage properties in polymer-coated Pd nanoparticles.[50] Other Pd composites include zeolites,[55] activated carbons,[56] polymers of intrinsic microporosity (PIMs),[57] and hyper-cross-linked polymers (HCPs),[58] with potential applications in heterogeneous catalysis as well.[59−61]

There is an increasing interest in the use of chemically synthesized, reusable metal nanoparticles to catalyze reactions with high activity and selectivity. Generally, metallic nanoparticles are functionalized with organic stabilizers (polymers, surfactants, or ligands) to prevent aggregation in solution and/or facilitate recycling of the catalyst.[62] In addition, the stabilizers play an essential role in controlling both the size and shape of the nanoparticle during the catalytic reaction.[63] Transition-metal nanoparticles have been widely used as catalysts either in solution or adsorbed on solid supports for various reactions, such as the hydrogenation of olefins.[60,62,64,65] Crooks and co-workers reported the use of dendrimer-encapsulated Pd nanoparticles for catalyzing the hydrogenation of olefins[66] and C−C coupling Heck[67] and Stille[68] reactions. They studied the effect of nanoparticle size on the hydrogenation of allyl alcohols[69] and developed a fluorous phase Pd-dendrimer catalyst that could be recycled and reused in multiple cycles.[65] Herrmann described the use of Pd nanoparticles stabilized with tetraoctylammonium bromide (TOABr) to catalyze Heck coupling reactions.[70] El-Sayed and co-workers reported the use of polyvinylpyrrolidone (PVP)-stabilized Pd nanoparticles in Suzuki coupling reactions.[71−73] Pd nanoparticles immobilized on resin,[74] silica,[75] or charcoal[76] were employed to perform the hydrogenation of conjugated dienes into monoolefins.

For applications in sensing, storage, and catalysis, it is clearly of interest to synthesize Pd nanomaterials that are highly reactive with hydrogen in a reversible manner and stable throughout many reaction cycles. This report describes results for Pd monolayer-protected clusters coated with mixed monolayers of $C8NH_2$ and C6S. As the $C8NH_2$/C6S ratio increases, the reactivity increases, but stability decreases. Importantly, we report the optimum ratio where both high reactivity and stability occurs based on optical measurements of mixed $C8NH_2$/C6S Pd MPCs in solution and electronic measurements of solid-state films. The results here represent a significant improvement over our previous work on single component Pd MPCs, since those materials suffered from either: (1) irreversible aggregation or morphology changes, (2) low, irreversible reactivity, (3) the need for pretreatment and/or significant conditioning for reversible hydrogen reactivity and sensing, (4) use only as solid-state films (not in solution), and (5) the presence of a large amount of excess surfactant during synthesis, which would need to be separated for applications in catalysis.

EXPERIMENTAL SECTION

Chemicals. Toluene (99.9%), 2-propanol (99.9%), acetonitrile (99%), and ethanol (200 proof) were purchased from VWR Scientific Products. Hexanethiol (95%), sodium borohydride (99%), and potassium tetrachloropalladate (II) (98%) were purchased from Aldrich Chemical Co. Tetraoctylammonium bromide (98%) and octylamine (99%) were purchased from Alfa Aesar Co. Barnstead nanopure water (18.3 MΩ-cm) was employed for all aqueous solutions.

Synthesis of Hexanethiolate-Coated Pd MPCs (C6S Pd MPCs). All glassware was cleaned in aqua regia (3:1, HCl:HNO_3) for at least 30 min (Caution: aqua regia is highly corrosive and should be handled with care under a fume hood.), thoroughly rinsed with deionized and nanopure water and acetone, and then dried at room temperature prior to use. Hexanethiolate-coated (C6S) Pd MPCs were synthesized as reported previously.[1,2,77,78] First, 0.53 g of K_2PdCl_4 was dissolved in 10 mL of water, and 1.32 g of TOABr was dissolved by sonication in 150 mL of toluene in a 250 mL Erlenmeyer flask. The two solutions were

then combined and stirred until the $PdCl_4^{2-}$ was transferred into the toluene phase, as indicated by the colorless toluene layer becoming deep red (~30 min). The colorless water layer was removed and discarded, and 114 μL of hexanethiol was added with stirring to the toluene solution in a 1:2 C6SH/Pd ratio. The solution was cooled in an ice bath for 30 min and removed before adding 0.61 g of $NaBH_4$ dissolved in 10 mL of water with stirring. The solution was stirred overnight, the water layer was removed, and the toluene removed by rotary evaporation keeping the temperature below 40 °C. The black Pd MPC product was suspended in 100 mL of acetonitrile and collected by vacuum filtration. The clusters were washed with an additional 100 mL of acetonitrile and 100 mL of ethanol before thoroughly drying and collecting. Toluene was added to the filter frit, and the soluble C6S Pd MPCs were collected in the filter flask. The toluene was removed by evaporation, and the solid collected. The average diameter of Pd MPCs prepared this way is 3.0 nm according to transmission electron microscopy (TEM) images and literature.[77]

Synthesis of Octylamine-Coated Pd MPCs ($C8NH_2$ Pd MPCs). Octylamine-coated Pd MPCs were synthesized according to our previous report.[2] Solutions of 0.50 g (1.54 mmol) of K_2PdCl_4 dissolved in 10 mL of water and 1.68 g (3.07 mmol) of TOABr dissolved in 70 mL of toluene were combined and stirred until all $PdCl_4^{2-}$ transferred into the toluene phase. Then, 2.8 mL of octylamine was added, and the solution rapidly stirred for 1 h. Next, 0.87 g of $NaBH_4$ dissolved in 10 mL of water was added to the two-phase solution while stirring. The solution was stirred overnight, the water layer removed, and the toluene layer removed by evaporation, keeping the temperature below 40 °C. The black Pd MPC product was suspended in 100 mL of acetonitrile and collected by vacuum filtration. The clusters were washed and collected as described for C6S Pd MCPs. The average diameter of the $C8NH_2$-coated Pd MPCs is 3.0 ± 0.8 nm, as determined previously by atomic force microscopy (AFM).[2]

Synthesis of Pd MPCs Coated with Mixed Monolayers of Hexanethiolates and Octylamines. Approximately 0.05 g of $C8NH_2$ Pd MPCs was dissolved in 5.0 mL of toluene before addition of a variable amount of C6SH (0 to 5.0 μL). The solution was stirred overnight (or 5 h for 5.0 μL C6SH), and the toluene layer removed by rotary evaporation. For optical experiments, the Pd MPC product was suspended in 50 mL of acetonitrile, collected by filtration with a syringe filter using a 0.2 μm PTFE membrane, and washed with 20 mL of acetonitrile and 10 mL of ethanol. Finally, the Pd MPCs were dissolved in 10 mL of toluene that was passed through the membrane. For sensing experiments, the Pd MPC product was suspended in 50 mL of acetonitrile, collected by filtration, and washed with an additional 60 mL of acetonitrile and 20 mL of ethanol on a filter frit. The filter frit was then rinsed with toluene to dissolve the soluble MPCs, and the solution concentrated by evaporation.

Electrode Devices. Two Au electrodes separated by 23 μm were fabricated in a clean room facility by photolithography on a Si/SiO_x substrate as described previously.[1,2,42,79,80] Wire leads were attached to the Au contact pads with Ag epoxy (cured 12 h, 80 °C), which was further insulated with an overlayer of Torr-seal epoxy (cured 12 h, 80 °C). The electrodes were cleaned by rinsing in acetone, ethanol, and 2-propanol before drying under N_2. The device was then placed in a UVO ozone cleaner (Jelight Company Inc., Irvine, CA) for 10 min prior to film deposition. Films containing C6S, $C8NH_2$, and mixed $C8NH_2$/C6S monolayer Pd MPCs were drop-cast deposited using 1−2 drops of a 10 mg/mL toluene solution, which leads to many multilayers of nanoparticles with film thicknesses well above the thickness of the electrodes.[2] The deposition of MPCs was carried out by placing the drop(s) onto a vertically hanging electrode device and allowing the solvent to evaporate under the fume hood.

Electronic Measurements. Electronic measurements were performed with a CH Instruments 660A (Austin, TX) electrochemical workstation operating in chronoamperometry (CA) mode. One electrode device lead was connected to the working electrode lead, and the other electrode was connected to both the counter and reference electrode leads. The current was monitored at a potential of 0.3 V, while the device was exposed to alternating flows of pure N_2 carrier gas and H_2 mixed with carrier gas. The H_2 concentration was varied by mixing H_2 and N_2 at different flow rates controlled by Cole Parmer flow meters located between the sample and the gas cylinders and operated by a three-way valve.[2] All samples were exposed to 100, 6.0, and 1.0% H_2 for 450 s to monitor the electronic response to H_2. Stable, reversible sensor devices were also tested in the presence of 9.6 to 0.3% H_2.

Spectroscopic Measurements. The optical properties of Pd MPCs were evaluated over the range of 300−900 nm using a Varian Cary 50 Bio UV−vis spectrophotometer. At room temperature, 2 or 3 drops of toluene solutions containing 10 mg/mL Pd MPCs were placed in a 1 cm path length quartz cuvette and diluted further with toluene. The baseline of each spectrum was corrected using the spectrum of the solvent (toluene). The absorbance spectrum of the solutions was measured following exposure to pure H_2 bubbling through the solution at a flow rate of 4.50 ± 0.12 mL/min for 0, 5, 15, 30, and 60 min. Pd MPCs synthesized within a day were used for these experiments to improve experiment reproducibility.

Other Characterization. After exposing a dilute toluene solution of C6S Pd MPCs or $C8NH_2$ Pd MPCs to 4.50 ± 0.12 mL/min H_2 for 60 min, the solution was sonicated for 2 min and drop-cast deposited onto a copper grid-supported holey carbon film for electron microscopy measurements. Images were obtained at different magnifications using a FEI Tecani F20 field-emission transmission electron microscope (TEM) operating at an accelerating voltage of 200 keV. Thermogravimetric analysis (TGA) data of pure C6S Pd and $C8NH_2$ Pd MPCs were obtained over a temperature range of 25−800 °C at a heating rate of 20 °C/min on a 2950 TGA HR V5.4A instrument under nitrogen (55, 75 mm scale), using sample sizes of 18.4−19.8 mg.

RESULTS AND DISCUSSION

Synthesis and Analysis of Pd MPCs. As described in the Experimental Section, we synthesized C6S Pd, $C8NH_2$ Pd, and mixed $C8NH_2$/C6S Pd MPCs. The average diameter of the C6S Pd and $C8NH_2$ Pd MPCs was 3.0 nm, which corresponds to 919 Pd atoms based on a simple spherical model. TGA of C6S Pd and $C8NH_2$ Pd MPCs (Figure S-1, Supporting Information) revealed that the MPCs contain 18.83 and 18.93% organic composition, respectively, giving average formulas of $Pd_{919}(C6S)_{192}$ and $Pd_{919}(C8NH_2)_{177}$. As illustrated in Scheme 1, we prepared different ratios of $C8NH_2$/C6S Pd MPCs by a liquid-phase place-exchange reaction between $C8NH_2$ Pd and free C6SH ligands in solution. The reaction proceeds as follows:

$$Pd_{919}(C8NH_2)_{177} + x\text{C6SH} \rightarrow Pd_{919}(C8NH_2)_{177-x}(C6S)_x + x\text{C8NH}_2 + 1/2x\text{H}_2 \quad (1)$$

We assume that the C6S ligands stoichiometrically replace the $C8NH_2$ ligands during this reaction since the Pd−S−R bond is much stronger compared to Pd−NH_2−R.[1,2] Nuclear magnetic resonance (NMR) spectroscopy of solutions of $C8NH_2$ Pd MPCs and C6SH supports this assumption. We also estimate the total number of ligands as 177, even though replacement of $C8NH_2$ with C6S could lead to a higher density of C6S ligands on the surface. Table 1 summarizes the synthesis of Pd MPCs with various $C8NH_2$/C6S ratios. The different Pd MPCs prepared include x = 0, 3, 10, 16, 32, and 81 and pure $Pd_{919}C6S_{192}$.

Scheme 1. Preparation of Mixed Monolayers of Hexanethiolate (C6S) and Octylamine ($C8NH_2$) Pd MPCs by Liquid-Phase Place Exchange

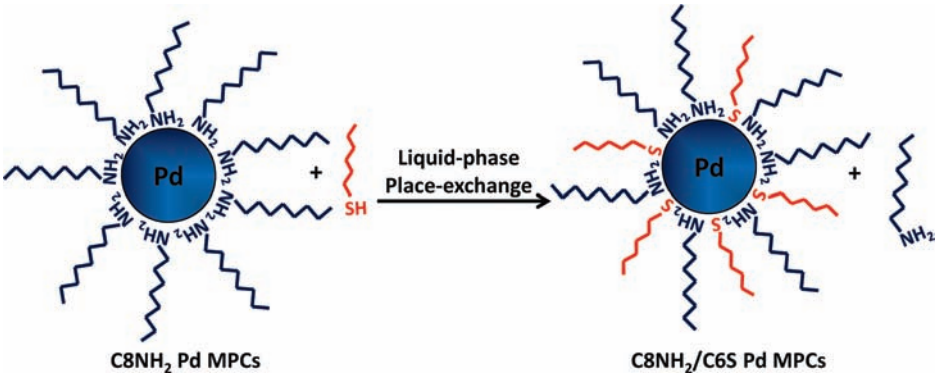

Table 1. Quantities of Reagents Used and Estimated Composition for $C8NH_2$/C6S Pd MPCs Synthesized by Place Exchange

mg $C8NH_2$ Pd	mol $C8NH_2$	μL C6SH	mol C6SH	Pd/$C8NH_2$/C6S
50.0	7.33×10^{-5}	0	0	919/177/0
50.8	7.45×10^{-5}	0.2	1.42×10^{-6}	919/174/3
50.1	7.35×10^{-5}	0.6	4.25×10^{-6}	919/167/10
49.8	7.30×10^{-5}	1.0	7.09×10^{-6}	919/161/16
49.7	7.29×10^{-5}	2.0	1.42×10^{-5}	919/145/32
50.0	7.33×10^{-5}	5.0	3.54×10^{-5}	919/96/81
C6S Pd	—	—	—	919/0/192

Overall, the compositions provided are rough estimates, and although Scheme 1 shows a random mixture of C6S and $C8NH_2$ ligands, phase segregation[81] of the ligands or preferential exchange at surface atom defects[82−84] could occur. In all cases, the solution of $C8NH_2$ Pd MPCs and C6SH was stirred overnight, except for the case where $x = 81$ (5.0 μL C6SH). In that case, we stirred the solution for only 5 h, since UV−vis data showed that Pd^0 converts to Pd(II) after longer stirring times (see Figure S-2, Supporting Information for more details).

Hydrogen Reactivity with C6S and $C8NH_2$ Pd MPCs. UV−vis spectroscopy and TEM imaging provided information about the reactivity and stability of Pd MPCs in solution in the presence of H_2 for different amounts of time, while films of Pd MPCs provided information on the reactivity in the solid state. Figure 1 shows normalized UV−vis spectra of diluted toluene solutions containing pure C6S Pd and $C8NH_2$ Pd MPCs, which were exposed to 100% H_2 at a constant flow of 4.50 ± 0.12 mL/min for 0, 5, 15, 30, and 60 min. The spectrum of the C6S Pd MPCs (Frame A) changed minimally after H_2 exposure over 60 min compared to the spectrum of the $C8NH_2$ Pd MPCs, which exhibited a dramatic absorbance decrease with time (Frame B). The loss in absorbance was accompanied by the noticeable precipitation of the $C8NH_2$ Pd MPCs, likely induced by the formation of PdH_x (see Figure S-3, Supporting Information for a picture of the precipitated Pd MPCs).

We used TEM to directly correlate the UV−vis data with the morphology of the Pd MPCs. Figure 2A and B shows TEM images of C6S Pd and $C8NH_2$ Pd MPCs before H_2 exposure, respectively, while Figure 2C and D shows the images of the corresponding samples after H_2 exposure. Before exposure, both

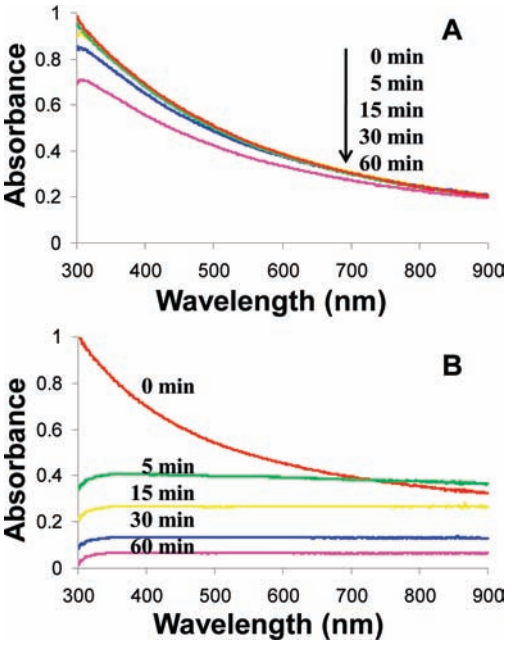

Figure 1. UV−vis spectra of a toluene solution of (A) C6S Pd MPCs and (B) $C8NH_2$ Pd MPCs before and after exposure to 100% H_2 at a flow rate of 4.50 mL/min for different times.

samples show the presence of metal nanoparticles in the expected 3.0 nm diameter size range. All of the C6S Pd MPCs are well-isolated and spherical (Frame A). In contrast, several of the $C8NH_2$ Pd MPCs appear oddly shaped or slightly aggregated (Frame B). Figure 2C and D show the TEM images of C6S Pd and $C8NH_2$ Pd MPCs, respectively, after exposure to 100% H_2 for 60 min at a constant flow of 4.50 ± 0.12 mL/min. The images of the C6S Pd MPCs show a few well-isolated nanoparticles and several that have undergone some aggregation. The extent of aggregation is similar to that of the $C8NH_2$ Pd MPCs before exposure to H_2 (Frame B). The image of the $C8NH_2$ Pd MPCs is dramatically different after H_2 exposure. All of the clusters aggregated into large superstructures with dimensions in the several hundred nanometer to micrometer size range. There was no evidence of individual, isolated nanoparticles in the images.

Figure 3 shows current−time (i−t) plots of films of pure C6S Pd and $C8NH_2$ Pd MPCs at a voltage of 0.3 V in 100% N_2

dx.doi.org/10.1021/ja108378x | J. Am. Chem. Soc. 2011, 133, 4389–4397

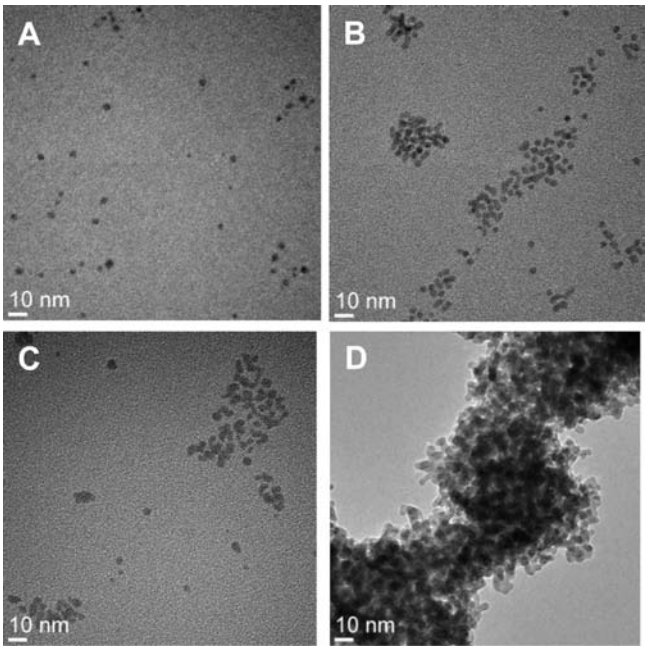

Figure 2. TEM images of drop-cast films of C6S Pd MPCs and $C8NH_2$ Pd MPCs before (A, B) and after exposure to 100% H_2 for 60 min (C, D).

initially from 0 to 50 s, then exposed to 100% H_2 (●) for 450 s and exposed back to 100% N_2 (▼) for 100 s. The current was stable for both films during the initial 100% N_2 exposure from 0 to 50 s. In the presence of 100% H_2 at 50 s, the current passing through the film of C6S Pd MPCs increased irreversibly from 1.36×10^{-8} to 1.64×10^{-8} A over the 450 s period. The plot appears flat in Figure 3 because of the large current scale, but there was a small increase in the current that did not return to baseline upon exposure back to N_2 at 500 s (see inset). In contrast, the current passing through the film of $C8NH_2$ Pd MPCs displayed a large irreversible four order of magnitude current increase from about 1.54×10^{-7} to 1.71×10^{-3} A upon exposure to 100% H_2 for 450 s.

The UV−vis, TEM, and electronic data consistently show that $C8NH_2$ Pd MPCs are much more reactive to H_2 compared to C6S Pd MPCs. The reaction between $C8NH_2$ Pd MPCs and H_2 presumably leads to the formation of PdH_x. The PdH_x formation leads to cluster aggregation, as evidenced by the decrease in absorbance with time, noticeable precipitation, and presence of large aggregated structures in the TEM images. Exposure to H_2 leads to strong Pd−H interactions, loss of the $C8NH_2$ ligands,[2] and cluster aggregation in solution. In the solid state, H_2 exposure to the film of $C8NH_2$ Pd MPCs leads to a large irreversible conductivity increase due to an irreversible film morphology change associated with Pd−H formation. The film morphology change leads to a more connected, lower resistance Pd film.[2] The TEM images also reveal that there was a small degree of aggregation of the $C8NH_2$ Pd MPCs even before H_2 exposure. This is again due to the weak Pd−NH_2 interactions, which leads to less stable clusters compared to those protected with C6S ligands. Further evidence of this is the fact that some $C8NH_2$ Pd MPCs eventually precipitate when stored in solution for more than a week, and they are generally not as stable when stored in solution or air compared to C6S Pd MPCs. The initial current of the film of $C8NH_2$ Pd MPCs was 1.54×10^{-7} A compared to 1.36×10^{-8} A for the film of C6S Pd MPCs. This is also consistent with the TEM images, which shows that the $C8NH_2$ Pd MPCs underwent some aggregation even before H_2 exposure. This likely led to the higher initial conductivity in the solid-state films.

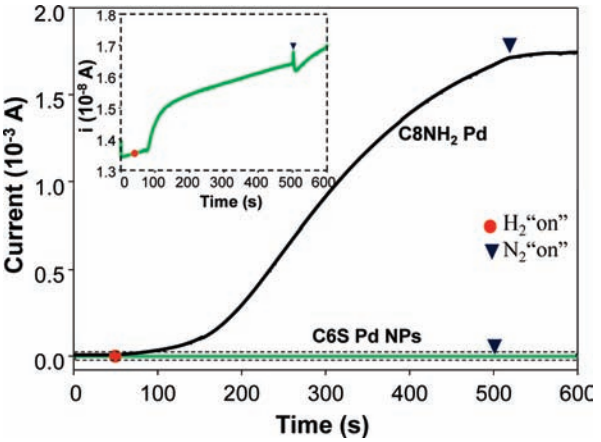

Figure 3. Current−time plots of drop-casted deposited films of C6S Pd (green plot) and $C8NH_2$ Pd MPCs (black plot) measured at 0.3 V during exposure to 100% H_2 (●) and 100% N_2 (▼) over a 450 s time period. (Inset) Expanded plot for the film of C6S Pd MPCs.

The small changes in the UV−vis spectra of the C6S Pd MPCs in the presence of H_2 shows that these clusters are much less reactive to H_2 or that they react with H_2 in a manner that does not lead to as much aggregation or morphology changes compared to $C8NH_2$ Pd MPCs. This is supported by the minimal change in the morphology of the MPCs shown in the TEM images after H_2 exposure. Both the UV−vis and TEM data consistently show that there is a small degree of aggregation of Pd MPCs resulting from the reaction between H_2 and C6S Pd MPCs. The small conductivity increase for solid-state films of C6S Pd MPCs after exposure to H_2 is also consistent with some reactivity with H_2. The irreversible conductivity increase could be due to the small degree of aggregation and morphology changes, as shown by the TEM images and UV−vis spectra or due to the inability of atomic H to combine and reform H_2 in the presence of the C6S ligands poisoning the Pd surface.[85,86]

Scheme 2 illustrates the differences between the reaction of H_2 with C6S Pd and $C8NH_2$ Pd MPCs. Based on the data, C6S Pd MPCs show little reactivity with H_2. Only a small amount of cluster aggregation or film morphology change occurs. In contrast, the $C8NH_2$ Pd MPCs readily react with H_2, which leads to a larger degree of cluster aggregation and film morphology changes accompanied by a large loss of the $C8NH_2$ ligands from the cluster surface, as shown by our group previously.[2] The H_2 does not readily react with C6S Pd MPCs since they are coated with a strong binding thiolate ligand. The Pd−H bond is likely inhibited by the Pd−S bonds. PdH_x can readily form on the $C8NH_2$ Pd MPCs because of the much weaker Pd−NH_2 interaction.

Hydrogen Reactivity with $C8NH_2$/C6S Mixed-Monolayer Pd MPCs. Figure 4 shows plots of the normalized absorbance at 310 nm of toluene solutions of $C8NH_2$ Pd, C6S Pd, and $C8NH_2$/C6S Pd MPCs of varied ratio as a function of exposure time to pure H_2 bubbling through the solution at a flow rate of 4.50 ± 0.12 mL/min. The points and curves represent the average of three samples prepared for each ratio with the standard deviations shown. The absorbance of $C8NH_2$ Pd MPCs decreased rapidly with time, almost reaching 0 after 60 min as also shown in Figure 1B. As the number of C6S ligands on the MPCs increased,

dx.doi.org/10.1021/ja108378x | J. Am. Chem. Soc. 2011, 133, 4389–4397

Scheme 2. Illustration of the Reactivity of (A) C6S Pd MPCs and (B) C8NH$_2$ Pd MPCs upon Exposure to 100% H$_2$

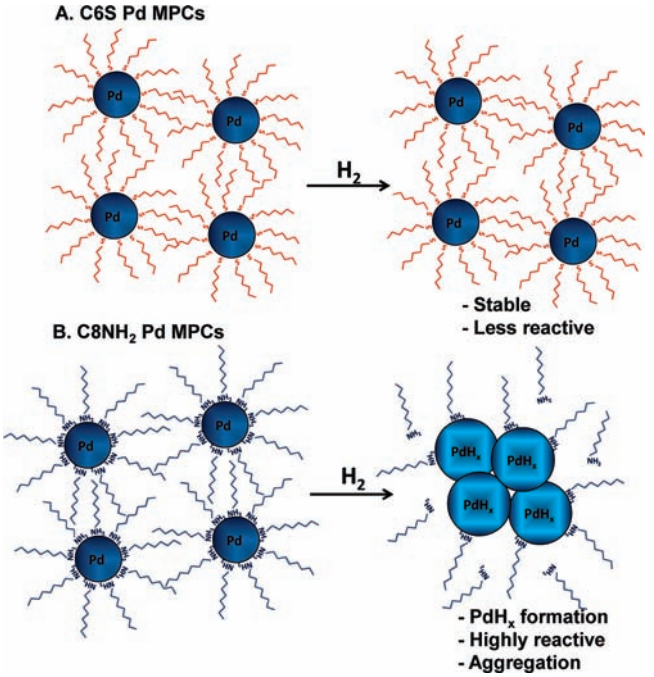

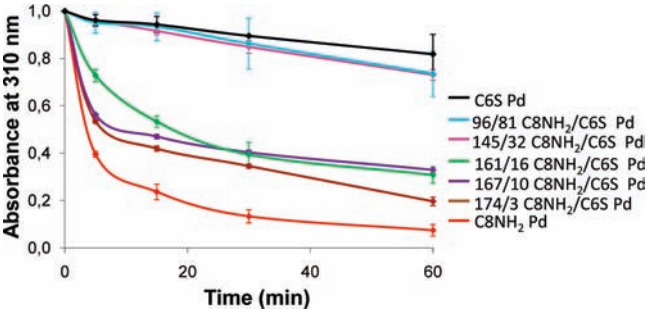

Figure 4. Plots of the normalized absorbance at 310 nm of toluene solutions containing C6S Pd, 96/81, 145/32, 161/16, 167/10, 174/3 C8NH$_2$/C6S Pd, and C8NH$_2$ Pd versus exposure time to 100% H$_2$ bubbling through the solutions at a flow rate of 4.50 ± 0.12 mL/min.

the rate of aggregation decreased, and the overall stability against aggregation increased. For C8NH$_2$/C6S ratios of 174/3, 167/10, and 161/16, the Pd MPCs displayed a stable absorbance at *A* ~0.2−0.4, showing that a little more than half of the Pd MPCs became insoluble. The normalized absorbance of the solutions of 145/32, 96/81, and pure C6S-coated Pd MPCs was stable at *A* ~0.8−0.9 after 60 min, indicating a small change in absorbance and high stability against aggregation in the presence of H$_2$. Assuming that the H$_2$ reactivity leads to aggregation, this suggests that less reactivity occurred.

The data in Figure 4 interestingly show that partial coverage with C6S ligands provides a large amount of stability against H$_2$-induced aggregation. Even with only 32 C6S ligands out of 177 total, the Pd MPCs were quite stable. It may be that there are only a limited number of reactive sites (edges and vertices, for example) on the Pd MPCs and that these sites are protected with a low C6S coverage. Others have shown that thiol place-

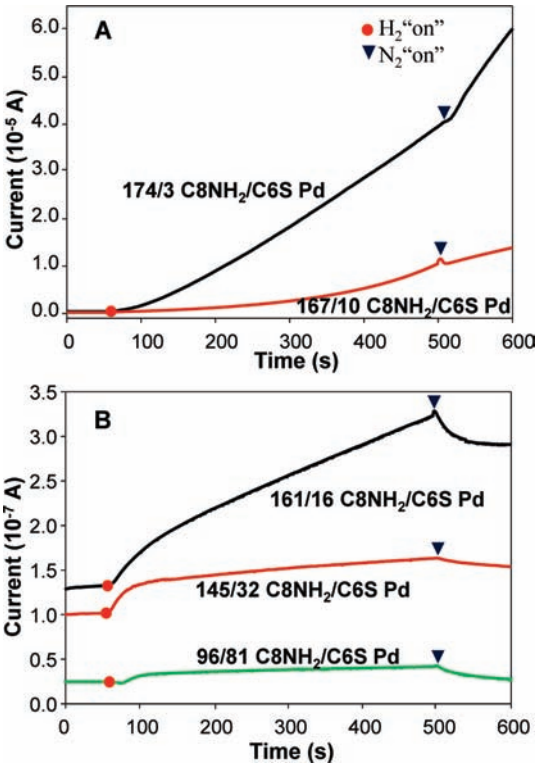

Figure 5. Current−time plots of drop-cast deposited films of (A) 174/3 and 167/10 and (B) 161/16, 145/32, and 96/81 C8NH$_2$/C6S Pd MPCs measured at 0.3 V during exposure to 100% H$_2$ (●) and 100% N$_2$ (▼) over a 600 s period.

exchange reactions occur preferentially at nanoparticle edge and vertex sites,[82−84] which might also be the most reactive sites for H$_2$ adsorption and subsequent aggregation of the PdH$_x$ MPCs. A 3.0 nm diameter nanoparticle shaped as a truncated octahedron has about 31% defect surface atoms (edge and vertex).[87] Covering the edge and vertex atoms would require an estimated 55 ligands out of the 177. This is larger than the Pd MPCs with 32 C6S ligands that showed high stability against H$_2$-induced aggregation but within range considering that our composition is an estimate.

Figure 5 displays current−time plots for films of C8NH$_2$/C6S Pd MPCs with various ratios as indicated in the presence of N$_2$ initially from 0 to 50 s, followed by exposure to 100% H$_2$ (●) for 450 s and finally exposed back to 100% N$_2$ (▼) for 100 s. Figure 5A shows that for a film of 174/3 C8NH$_2$/C6S Pd MPCs, the current increased irreversibly from about 4.06 × 10^{-7} to 4.06 × 10^{-5} A. Similarly, the current through the film of 167/10 Pd MPCs increased from 1.91 × 10^{-7} to 1.05 × 10^{-5} A upon exposure to 100% H$_2$. The current increase is due to irreversible aggregation of the Pd MPCs upon PdH$_x$ formation and removal. Interestingly, this is significantly smaller than the four order of magnitude increase observed for pure C8NH$_2$ Pd films in Figure 3. The presence of a low coverage of C6S ligands (x = 3−10) leads to a smaller current increase in the film following the 100% H$_2$ exposure, but it is still significant. This is consistent with a smaller amount of H$_2$-induced aggregation for Pd MPCs with 3−10 C6S ligands compared to pure C8NH$_2$ Pd MPCs, as observed in the spectroscopy studies (Figure 4).

Figures 5B shows the current−time plot of films of 161/16, 145/32, and 96/81 C8NH$_2$/C6S Pd MPCs upon exposure to

dx.doi.org/10.1021/ja108378x |*J. Am. Chem. Soc.* 2011, 133, 4389–4397

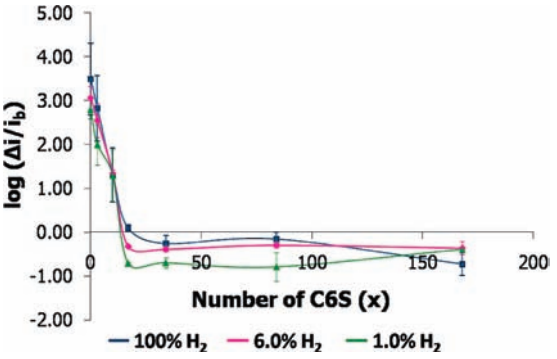

Figure 6. The log of the relative change in current of Pd MPCs exposed to different H_2 concentration for 450 s followed by N_2 for 100 s.

100% H_2. The current increased by approximately 3 or 2 times (1.32×10^{-7} to 3.22×10^{-7} A, 1.02×10^{-7} to 1.63×10^{-7} A, and 2.46×10^{-8} to 4.17×10^{-8} A, respectively) following exposure to 100% H_2, which is dramatically less compared to the 2−4 order of magnitude current increase observed with x = 0−10 C6S ligands. Another major difference between the Pd MPC films with 0−10 C6S ligands compared to those with 16−81 C6S ligands is that the current continued to increase in the presence of N_2 following the exposure to 100% H_2 for the former and that the current decreased back toward the original baseline current for the latter. The morphology of the film continues to change in the presence of N_2, even after H is removed from Pd for the films of Pd MPCs with 0−10 C6S ligands. The films of Pd MPCs with 16−81 ligands, in contrast, remain stable and exhibit more reversibility during H insertion and removal from Pd. Films of 96/81 C8NH_2/C6S Pd MPCs, in particular, displayed a fairly stable current increase during the 450 s exposure to H_2 and then exhibited a decrease in current close to the baseline upon subsequent N_2 exposure.

We quantified the current change exhibited by films of Pd MPCs coated with C8NH_2, C6S, and mixed C8NH_2/C6S upon initial exposure to different H_2 concentrations. We calculated the relative change in current by the equation:

$$\Delta i_{\text{relative}} = (i_r - i_b)/i_b = \Delta i/i_b$$

where i_b is the initial baseline current in 100% N_2, i_r is the current in the presence of the H_2/N_2 mixture after 450 s, and $\Delta i = (i_r - i_b)$. Figure 6 shows the log of the relative change in current as a function of the varied composition of (C8NH_2/C6S)-coated Pd MPCs after exposure to 1.0, 6.0, and 100% H_2 for a period of 450 s and subsequent exposure to 100% N_2 for 100 s. The points represent the average of several samples prepared for each ratio with the standard deviations also shown. When x = 0−10 C6S ligands, the Pd MPCs were highly reactive to 1.0, 6.0, and 100% H_2, as indicated by the large irreversible 2−4 order of magnitude increase in current. Films of pure C6 Pd MPCs (x = 192 C6S ligands) were not highly reactive to H_2, as determined by minimal changes in resistance in the presence of H_2 at different concentrations (log[response] ~ −1). When x = 16−81 C6S ligands, the Pd MPCs exhibited a slightly larger current response to H_2 compared to pure C6S Pd MPCs but not as large as those with fewer C6S ligands (x = 0−10). More importantly, the films of these Pd MPCs were fairly stable and showed a somewhat reversible change in current in the presence of H_2.

Figure 7 displays current−time plots for a film of 96/81 C8NH_2/C6S Pd MPCs in the presence of 100% N_2 initially and then exposed to 1.0% H_2 (Frame A) and various concentrations

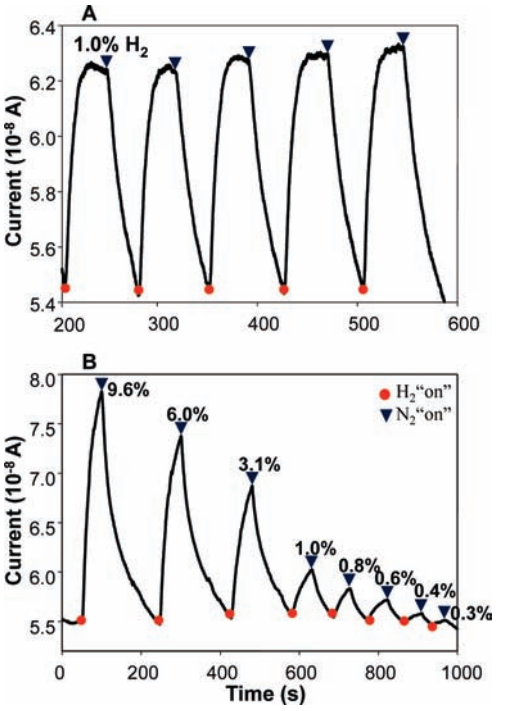

Figure 7. Current−time plots of a film of 96/81 C8NH_2/C6S Pd MPCs exposed to (A) 100% N_2 (▼) and 1.0% H_2 (●) for five cycles, and (B) 100% N_2 (▼) and 9.6−0.3% H_2 (●).

of H_2 (Frame B). Figure 7A shows the high reversibility of a film of 96/81 C8NH_2/C6S Pd MPCs following alternating exposure to 1.0% H_2 (●) and 100% N_2 (▼) for five cycles. The current through the film quickly increased by a factor of 1.2 (from about 5.46×10^{-8} to about 6.24×10^{-8} A) in the presence of H_2 and reversibly returned close to its original value upon exposure back to 100% N_2. This result indicates that films containing 96/81 C8NH_2/C6S Pd MPCs are responsive reversibly to H_2. They are also highly stable against aggregation and large morphology changes, as indicated by UV−vis data for solutions of the MPCs.

Figure 7B shows a current−time plot for a film of 96/81 C8NH_2/C6S Pd MPCs that was exposed to H_2 concentrations from 9.6% down to 0.3% H_2. The film was initially exposed to 100% N_2 and then exposed to cycles of various concentrations of H_2 (●) and 100% N_2 (▼). The sensing experiment in Figure 7B occurred after some conditioning of the film until it displayed the reversible behavior shown in Figure 7A. Figure 7B shows that the film of 96/81 C8NH_2/C6S Pd MPCs exhibited a reversible increase in current in the presence of 9.6−0.3% H_2. The increase in current was likely due to the volume enhancement of the Pd MPCs upon PdH_x formation, which lowers the resistance between the Pd MPCs in the film. The Supporting Information (Figure S-4) shows the calibration curve, where the experimental detection limit is about 0.3% H_2. Because of the stability and the relatively fast and reversible response to H_2 over a range of concentrations, these Pd MPCs are not only potentially useful for H_2 sensing but also excellent candidates for H_2 storage and catalysis studies involving H_2 as a reactant.

■ CONCLUSIONS

We synthesized pure C8NH_2 Pd and C6S Pd and mixed monolayer C8NH_2/C6S Pd MPCs with varying C8NH_2/C6S

dx.doi.org/10.1021/ja108378x |J. Am. Chem. Soc. 2011, 133, 4389–4397

ratios by a liquid-phase place-exchange method and compared their reactivity and stability to H_2 gas by UV−vis spectroscopy, TEM, and electronic conductivity measurements. While $C8NH_2$ Pd MPCs are highly reactive, they are not stable in the presence of H_2 since they irreversibly aggregate. C6S Pd MPCs are highly stable but only react minimally with H_2 based on UV−vis and conductivity data. Mixed monolayer $C8NH_2$/C6S Pd MPCs show properties intermediate of the two pure Pd MPCs. The reactivity and stability strongly depend on the $C8NH_2$/C6S ratio of the mixed monolayers on the Pd MPCs. At high ratios (x = 3−16 C6S ligands), the Pd MPCs behave similarly to the pure $C8NH_2$ Pd MPCs, although they are slightly more stable. At medium ratios (x = 32 and 81 C6S ligands), the Pd MPCs are fairly stable based on UV−vis data of solutions and show reversible reactivity to H_2 based on reversible increases in current for solid-state films in the presence of H_2. This was particularly evident for the 96/81 $C8NH_2$/C6S Pd MPCs, which showed excellent stability against H_2-induced aggregation in solution and a reversible electronic response to H_2 for at least five cycles and down to 0.3% H_2 as solid-state films. These are the most promising for sensing, storage, and catalysis applications. Future experiments will explore the details of H_2 sensing and catalysis applications of these interesting materials.

■ ASSOCIATED CONTENT

Supporting Information. TGA of C6S Pd and $C8NH_2$ Pd MPCs, UV−vis data of Pd MPCs coated with different ratios of ligands, digital photo of diluted solutions of C6S Pd and $C8NH_2$ Pd MPCs before and after H_2 bubbling for 60 min at a constant flow of 4.50 ± 0.12 mL/min, and H_2 sensing calibration curve. This material is available free of charge via the Internet at http://pubs.acs.org.

■ AUTHOR INFORMATION

Corresponding Author
f.zamborini@louisville.edu

■ ACKNOWLEDGMENT

We gratefully acknowledge the Kentucky Science and Engineering Foundation (KSEF-2012-RDE-012) for financial support of this research. We thank Kevin Walsh and Mark M. Crain from the Department of Electrical and Computer Engineering at the University of Louisville for the microfabricated electrode devices. We also thank the Conn Center for Renewable Energy Research for use of the TGA and TEM facilities.

■ REFERENCES

(1) Ibañez, F. J.; Zamborini, F. P. *Langmuir* **2006**, *22*, 9789–9796.
(2) Ibañez, F. J.; Zamborini, F. P. *J. Am. Chem. Soc.* **2008**, *130*, 622–633.
(3) Chiu, S.-Y.; Huang, H.-W.; Huang, T.-H.; Liang, K.-C.; Liu, K.-P.; Tsai, J.-H.; Lour, W.-S. *Sens. Actuators, B* **2009**, *138*, 422–427.
(4) Manjula, P.; Satyanarayana, L.; Swarnalatha, Y.; Manorama, S. V. *Sens. Actuators, B* **2009**, *138*, 28–34.
(5) Lin, H.; Gao, T.; Fantini, J.; Sailor, M. J. *Langmuir* **2004**, *20*, 5104–5108.
(6) Balat, M. *Int. J. Hydrogen Energy* **2008**, *33*, 4013–4029.
(7) RaviPrakash, J.; McDaniel, A. H.; Horn, M.; Pilione, L.; Sunal, P.; Messier, R.; McGrath, R. T.; Schweighardt, F. K. *Sens. Actuators, B* **2007**, *120*, 439–446.
(8) Schlapbach, L.; Züttel, A. *Nature* **2001**, *414*, 353–358.
(9) Kumar, M. K.; Ramaprabhu, S. *Int. J. Hydrogen Energy* **2007**, *32*, 2518–2526.
(10) Murray, L. J.; Dincă, M.; Long, J. R. *Chem. Soc. Rev.* **2009**, *38*, 1294–1314.
(11) Lewis, F. A. *The Palladium/Hydrogen System*; Academic Press Inc.: London, 1967.
(12) Jia, W.; Su, L.; Ding, Y.; Schempf, A.; Wang, Y.; Lei, Y. *J. Phys. Chem. C* **2009**, *113*, 16402–16407.
(13) Kim, C.; Kim, Y. A.; Kim, J. H.; Kataoka, M.; Endo, M. *Nanotechnology* **2008**, *19*, 145602 (5pp).
(14) Hakamada, M.; Nakano, H.; Furukawa, T.; Takahashi, M.; Mabuchi, M. *J. Phys. Chem. C* **2010**, *114*, 868–873.
(15) Christofides, C.; Mandelis, A. *J. Appl. Phys.* **1990**, *68*, 1–30.
(16) Smith, A. L.; Shirazi, H. M. *Thermochim. Acta* **2005**, *432*, 202–211.
(17) Robinson, J. A.; Snow, E. S.; Bădescu, Ş. C.; Reinecke, T. L.; Perkins, F. K. *Nano Lett.* **2006**, *6*, 1747–1751.
(18) Kolmakov, A.; Klenov, D. O.; Lilach, Y.; Stemmer, S.; Moskovits, M. *Nano Lett.* **2005**, *5*, 667–673.
(19) Staii, C.; Johnson, A. T., Jr.; Chen, M.; Gelperin, A. *Nano Lett.* **2005**, *5*, 1774–1778.
(20) Salehi, A.; Nikfarjam, A. *Sens. Actuators, B* **2004**, *101*, 394–400.
(21) Dankert, O.; Pundt, A. *Appl. Phys. Lett.* **2002**, *81*, 1618–1620.
(22) Favier, F.; Walter, E. C.; Zach, M. P.; Benter, T.; Penner, R. M. *Science* **2001**, *293*, 2227–2231.
(23) Kaltenpoth, G.; Schnabel, P.; Menke, E.; Walter, E. C.; Grunze, M.; Penner, R. M. *Anal. Chem.* **2003**, *75*, 4756–4765.
(24) Kang, W. P.; Gürbüz, Y. *J. Appl. Phys.* **1994**, *75*, 8175–8181.
(25) Kong, J.; Chapline, M. G.; Dai, H. *Adv. Mater.* **2001**, *13*, 1384–1386.
(26) Luongo, K.; Sine, A.; Bhansali, S. *Sens. Actuators, B.* **2005**, *111*−*112*, 125–129.
(27) Mizsei, J.; Voutilainen, J.; Saukko, S.; Lantto, V. *Thin Solid Films* **2001**, *391*, 209–215.
(28) Morris, J. E.; Kiesow, A.; Hong, M.; Wu, F. *Int. J. Electronics* **1996**, *81*, 441–447.
(29) Sakamoto, Y.; Takai, K.; Takashima, I.; Imada, M. *J. Phys: Condens. Matter* **1996**, *8*, 3399–3411.
(30) Sayago, I.; Terrado, E.; Lafuente, E.; Horrillo, M. C.; Maser, W. K.; Benito, A. M.; Navarro, R.; Urriolabeitia, E. P.; Martinez, M. T.; Gutierrez, J. *Synth. Met.* **2005**, *148*, 15–19.
(31) Walter, E. C.; Favier, F.; Penner, R. M. *Anal. Chem.* **2002**, *74*, 1546–1553.
(32) Xu, T.; Zach, M. P.; Xiao, Z. L.; Rosenmann, D.; Welp, U.; Kwok, W. K.; Crabtree, G. W. *Appl. Phys. Lett.* **2005**, *86*, 203104−1–203104−3.
(33) Yu, S.; Welp, U.; Hua, L. Z.; Rydh, A.; Kwok, W. K.; Wang, H. H. *Chem. Mater.* **2005**, *17*, 3445–3450.
(34) Yun, M.; Myung, N. V.; Vasquez, R. P.; Lee, C.; Menke, E.; Penner, R. M. *Nano Lett.* **2004**, *4*, 419–422.
(35) Kalli, K.; Othonos, A.; Christofides, C. *J. Appl. Phys.* **2002**, *91*, 3829–3840.
(36) Lin, H.; Gao, T.; Fantini, J.; Sailor, M. J. *Langmuir* **2004**, *20*, 5104–5108.
(37) Zhao, Z.; Carpenter, M. A. *J. Appl. Phys.* **2005**, *97*, 124301−1–124301−7.
(38) Zhao, Z.; Sevryugina, Y.; Carpenter, M. A.; Welch, D.; Xia, H. *Anal. Chem.* **2004**, *76*, 6321–6326.
(39) Sun, Y.; Wang, H. H.; Xia, M. *J. Phys. Chem. C* **2008**, *112*, 1250–1259.
(40) Jeon, K. J.; Lee, J. M.; Lee, E. Lee, W. *Nanotechnology* **2009**, *20*, 135502 (5 pp).
(41) Yang, F.; Taggart, D. K.; Penner, R. M. *Nano Lett.* **2009**, *9*, 2177–2182.
(42) Dasari, R.; Zamborini, F. P. *J. Am. Chem. Soc.* **2008**, *130*, 16138–16139.

(43) Chen, H.-I.; Chou, Y.-I.; Hsiung, C.-K. *Sens. Actuators, B* **2003**, *92*, 6–16.
(44) Hatakeyama, Y.; Umetsu, M.; Ohara, S.; Kawadai, F.; Takami, S.; Naka, T.; Adshiri, T. *Adv. Mater.* **2008**, *20*, 1122–1128.
(45) Sandrock, G. *J. Alloys Compd.* **1999**, *293*, 295–877.
(46) Kishore, S.; Nelson, J. A.; Adair, J. H.; Eklund, P. C. *J. Alloys Compd.* **2005**, *389*, 234–242.
(47) Langhammer, C.; Zorić, I.; Kasemo, B. *Nano Lett.* **2007**, *7*, 3122–3127.
(48) Rather, S.; Zacharia, R.; Hwang, S. W.; Naik, M.; Nahm, K. S. *Chem. Phys. Lett.* **2007**, *438*, 78–84.
(49) Wagemans, R. W. P.; van Lenthe, J. H.; de Jongh, P. E.; Jos van Dillen, A.; de Jong, K. P. *J. Am. Chem. Soc.* **2005**, *127*, 16675–16680.
(50) Yamauchi, M.; Ikeda, R.; Kitagawa, H.; Takata, M. *J. Phys. Chem. C* **2008**, *112*, 3294–3299.
(51) Yamauchi, M.; Kobayashi, H.; Kitagawa, H. *ChemPhysChem* **2009**, *10*, 2566–2576.
(52) Férey, G. *Chem. Soc. Rev.* **2008**, *37*, 191–214.
(53) Zlotea, C.; Campesi, R.; Cuevas, F.; Leroy, E.; Dibandjo, P.; Volkringer, C.; Loiseau, T.; Férey, G.; Latroche, M. *J. Am. Chem. Soc.* **2010**, *132*, 2991–2997.
(54) Hasell, T.; Wood, C. D.; Clowes, R.; Jones, J. T. A.; Khimyak, Y. Z.; Adams, D. J.; Cooper, A. I. *Chem. Mater.* **2010**, *22*, 557–564.
(55) Caro, J.; Noack, M.; Kolsch, P.; Schafer, R. *Microporous Mesoporous Mater.* **2000**, *38*, 3–24.
(56) Villar-Rodil, S.; Suarez-Garcia, F.; Paredes, J. I.; Martinez-Alonso, A.; Tascon, J. M. D. *Chem. Mater.* **2005**, *17*, 5893–5908.
(57) Carta, M.; Msayib, K. J.; Budd, P. M.; McKeown, N. B. *Org. Lett.* **2008**, *10*, 2641–2643.
(58) Lee, J. Y.; Wood, C. D.; Bradshaw, D.; Rosseinsky, M. J.; Cooper, A. I. *Chem. Commun.* **2006**, *25*, 2670–2672.
(59) Jiang, J. X.; Su, F.; Trewin, A.; Wood, C. D.; Niu, H.; Jones, J. T. A.; Khimyak, Y. Z.; Cooper, A. I. *J. Am. Chem. Soc.* **2008**, *130*, 7710–7720.
(60) Solodenko, W.; Wen, H. L.; Leue, S.; Stuhlmann, F.; Sourkouni-Argirusi, G.; Jas, G.; Schönfeld, H.; Kunz, U.; Kirschning, A. *Eur. J. Org. Chem.* **2004**, *17*, 3601–3610.
(61) Ma, L.; Abney, C.; Lin, W. *Chem. Soc. Rev.* **2009**, *38*, 1248–1256.
(62) Roucoux, A.; Schulz, J.; Patin, H. *Chem. Rev.* **2002**, *102*, 3757–3778.
(63) Durand, J.; Teuma, E.; Gómez, M. *Eur. J. Inorg. Chem.* **2008**, 3577–3586.
(64) Borsla, A.; Wilhelm, A. M.; Delmas, H. *Catal. Today* **2001**, *66*, 389–395.
(65) Chechik, V.; Crooks, R. M. *J. Am. Chem. Soc.* **2000**, *122*, 1243–1244.
(66) Wilson, O. M.; Knecht, M. R.; Garcia-Martinez, J. C.; Crooks, R. M. *J. Am. Chem. Soc.* **2006**, *128*, 4510–4511.
(67) Yeung, L. K.; Crooks, R. M. *Nano Lett.* **2001**, *1*, 14–17.
(68) Garcia-Martinez, J. C.; Lezutekong, R.; Crooks, R. M. *J. Am. Chem. Soc.* **2005**, *127*, 5097–5103.
(69) Niu, Y.; Yeung, L. K.; Crooks, R. M. *J. Am. Chem. Soc.* **2001**, *123*, 6840–6846.
(70) Beller, M.; Fischer, H.; Kühlein, K.; Reisinger, C.-P.; Herrmann, W. A. *J. Organomet. Chem.* **1996**, *520*, 257–259.
(71) Li, Y.; Hong, X. M.; Collard, D. M.; El-Sayed, M. A. *Org. Lett.* **2000**, *2*, 2385–2388.
(72) Narayanan, R.; El-Sayed, M. A. *J. Am. Chem. Soc.* **2003**, *125*, 8340–8347.
(73) Narayanan, R.; El-Sayed, M. A. *J. Phys. Chem. B* **2005**, *109*, 12663–12676.
(74) Hirai, H.; Yakura, N.; Seta, Y.; Hodoshima, S. *React. Funct. Polym.* **1998**, *37*, 121–131.
(75) Wang, Y.; Liu, H. *Polym. Bull.* **1991**, *25*, 139–144.
(76) Gittins, D. I.; Caruso, F. *Angew. Chem., Int. Ed.* **2001**, *40*, 3001–3004.
(77) Zamborini, F. P.; Gross, S. M.; Murray, R. W. *Langmuir* **2001**, *17*, 481–487.
(78) Brust, M.; Walker, M.; Bethell, D.; Schiffrin, D. J.; Whyman, R. *Chem. Commun.* **1994**, *7*, 801–802.
(79) Ibañez, F. J.; Zamborini, F. P. *ACS Nano* **2008**, *2*, 1543–1552.
(80) Ibañez, F. J.; Growrishetty, U.; Crain, M. M.; Walsh, K. M.; Zamborini, F. P. *Anal. Chem.* **2006**, *78*, 753–761.
(81) Singh, C.; Ghorai, P. K.; Horsch, M. A.; Jackson, A. M.; Larson, R. G.; Stellacci, F.; Glotzer, S. C. *Phys. Rev. Lett.* **2007**, *99*, 226106−1–226106−4.
(82) Hostetler, M. J; Templeton, A. C.; Murray, R. W. *Langmuir* **1998**, *15*, 3782–3789.
(83) Beeram, S. R.; Zamborini, F. P. *J. Am. Chem. Soc.* **2009**, *131*, 11689–11691.
(84) Beeram, S. R.; Zamborini, F. P. *ACS Nano* **2010**, *4*, 3633–3646.
(85) Kimura, A.; Birnbaum, H. K. *Acta Metall. Mater.* **1991**, *39*, 295–301.
(86) Gao, L; Conway, B. E. *Electrochim. Acta* **1994**, *39*, 1681–1693.
(87) Hostetler, M. J.; Wingate, J. E.; Zhong, C.-J.; Harris, J. E.; Vachet, R. W.; Clark, M. R.; Londono, J. D.; Green, S. J.; Stokes, J. J.; Wignall, G. D.; Glish, G. L.; Porter, M. D.; Evans, N. D.; Murray, R. W. *Langmuir* **1998**, *14*, 17–30.